A 5.12-12.95GHz Triple-Resonance Low Phase Noise CMOS VCO for Software-Defined Radio Applications

M. Moslehi Bajestan and K. Entesari

Analog and Mixed Signal Center, Texas A&M University, CS, TX, 77843, USA

***Abstract* — This paper presents a wide-tuning range Voltage-Controlled Oscillator (VCO) for software-defined radio (SDR) applications using a resonator with three potential oscillation modes. The implemented prototype in 0.18µm CMOS technology achieves a continuous tuning range of 86.7% from 5.12GHz to 12.95GHz while drawing 5 to 10mA current from 1-V supply. The measured phase noise at 1MHz offset from carrier frequencies of 5.9, 9.12 and 12.25GHz is -122.9, -117.1 and -110.5dBc/Hz, respectively. The VCO occupies a chip area of 0.33mm^2.**

***Index Terms* — Low phase noise, multi-band, software-defined radio, voltage-controlled oscillator, wide tuning range.**

I. Introduction

In recent years, there has been a growing interest toward multi-standard transceivers covering a large number of frequency bands such as Software Defined Radios (SDR). One of the key building blocks in an SDR is the local oscillator which needs to generate the quadrature signals from 100MHz to 6GHz while meeting the stringent phase noise performance requirements (considering direct-conversion architecture) [1]. Moreover, the oscillator needs to consume low power and have a compact size.

By employing a 6-12GHz VCO and a chain of divide-by-2 circuits, all the necessary quadrature signals for an SDR can be generated [1]. A single-tank LC VCO relying on only switched capacitor technique cannot cover such a wide frequency range while satisfying the required phase noise performance. Alternatively, multiple VCOs can be employed. However, this technique requires large silicon area and therefore increases the cost. Other techniques have been reported to widen the oscillator tuning range including VCOs exploiting switched inductors [2] and coupled inductors [3]-[6]. The VCOs based on switched inductors suffer from poor phase noise performance due to the loss of the switches inside the tank. On the other hand, in the VCOs with coupled inductors, the multi-oscillation modes of the resonator are employed to make a multi-band oscillator without using lossy switches to achieve better phase noise performance and more compact layout.

In a dual-band VCO with a 4th-order resonator (two coupled LC tanks) in [3], to cover a frequency range of 6-12GHz, the required tuning range in each band needs to be ~40-50%. However, such a tuning range is still very difficult to achieve, especially at higher frequencies because of the trade-offs between phase noise, tuning range and power dissipation. In this paper, another oscillation mode is added to a 4th-order resonator by properly placing an inductor between the two coils of the transformer to realize a triple-band VCO. This extra mode is employed to alleviate the aforementioned trade-offs and to improve the phase noise performance by reducing the required capacitance variations in each band. The modified resonator still maintains two potential resonant modes at each port. This property results in a simple method of switching between the three resonance frequencies which is robust to process, voltage and temperature (PVT) variations.

II. VCO Architecture

A. Proposed Resonator

Fig. 1(a) shows a dual-mode resonator composed of two magnetically coupled LC tanks. For this structure, assuming L_1=L_2=L and C_1=C_2=C, the two oscillation frequencies can be found as [5]

$$\omega_{even}{}^2 = \frac{\omega_o{}^2}{1+k}\ , \qquad \omega_{odd}{}^2 = \frac{\omega_o{}^2}{1-k} \tag{1}$$

where $\omega_o = 1/(\sqrt{LC})$ is the resonance frequency of the un-coupled tanks. In an attempt to add one more oscillation mode to this structure, another inductor (L_3) is placed at the line of symmetry where it has the same mutual coupling to L_1 and L_2 (Fig. 1(b)). The value of L_3 (L') is chosen such that together with C it has an individual resonance frequency of $\omega_o' = 1/(\sqrt{L'C})$ higher than ω_{odd}. As will be shown, the new resonator provides three resonant modes while only two of them appear at each port.

Assuming high-Q components, the input impedance at each port of the resonator can be derived as

$$Z_{11}(s) = Z_{22}(s) = \frac{N(s)}{D(s)}\ , \quad Z_{33}(s) = \frac{N'(s)}{D(s)} \tag{2}$$

$$N(s) = \frac{s}{C}\left[\left(1-k\right)\left(1+k-2k'^2\right)s^4 + \left(\omega_o{}^2\left(1-k'^2\right) + \omega_o{}'^2\left(1-k^2\right)\right)s^2 + \left(\omega_o\omega_o'\right)^2\right]$$

$$N'(s) = \frac{s}{C}\left[\left(1-k\right)s^2 + \omega_o{}^2\right]\left[\left(1+k-2k'^2\right)s^2 + \omega_o{}^2\right]$$

$$D(s) = \left[\left(1-k\right)s^2 + \omega_o{}^2\right]\left[\left(1+k-2k'^2\right)s^4 + \left(\omega_o{}^2 + \omega_o{}'^2\left(1+k\right)\right)s^2 + \left(\omega_o\omega_o'\right)^2\right]$$

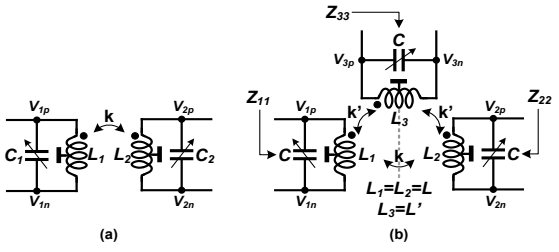

Fig. 1. (a) A dual-mode resonator, and (b) the proposed resonator.

Therefore, the resonator has three possible oscillation frequencies. The roots of the first term in $D(s)$ determine the middle-frequency resonance (ω_M) of the system while the roots of the last term correspond to the lower and higher- frequency resonances (ω_L and ω_H).

Interestingly, ω_M is equal to ω_{odd} which implies that the addition of L_3 does not affect the operation of the 4th-order resonator in its odd mode. Moreover, one of the notch frequencies in Z_{33} is located exactly at ω_M, hence, looking into port-3, the system potentially has only two resonance frequencies at ω_L and ω_H. Similarly, it can be easily shown that one of the notches of Z_{11} (Z_{22}) in (2) is located at a frequency very close to ω_H so by looking into port-1 (port-2), effectively two possible oscillation frequencies at ω_L and ω_M can be seen.

These results could be also deduced in an intuitive way. As an example, when the resonator is working at ω_M, the currents flowing through L_1 and L_2 have the same amplitude and are 180° out of phase. As a result, since $k_{13}=k_{23}=k'$, the two induced currents in L_3 will cancel out each other and it is like that this inductor does not exist in the system. Consequently, the resonance frequency of this mode (ω_M) will be equal to ω_{odd} and looking into port-3, no oscillation can occur at ω_M.

Based on the same analysis, only two dominant resonance peaks exist in the amplitude responses of Z_{12}, Z_{13} and Z_{23}. The peak frequencies of Z_{12} are located at ω_L and ω_M while the peaks of Z_{13} and Z_{23} are at ω_L and ω_H.

In summary, by placing an LC tank at the line of symmetry of a 4th-order resonator another resonant mode is added to the system. However, this extra mode can be only seen at port-3 and looking into port-1 and port-2, the resonator still maintains its dual-mode operation. This property of the resonator results in a simple and yet robust method for selecting the desired mode of oscillation.

B. Mode Switching

Fig. 2 shows the detailed schematic of the proposed triple-band VCO. The G_m-cells in this figure are employed to excite the desired mode of operation.

As shown in Fig. 3(a), there are only two dominant peaks in the amplitude response of Z_{12} located at ω_L and ω_M. Furthermore, the phase shift of Z_{12} is 0° at ω_L while it becomes -180° at ω_M. As a result, by placing a sufficiently positive or negative transconductance between L_1 and L_2, the oscillation condition at either ω_L or ω_M can be satisfied, respectively. Consequently, as illustrated in Fig. 2, to make the oscillator work at ω_L (ω_M), G_{m12} (G_{m21}) is turned on while the other G_m-cells are remained off. Moreover, in order to ensure the start-up of the oscillation, the values of G_{m12} and G_{m12} must satisfy the following conditions [3]

$$G_{m12} > \frac{1}{|Z_{12}|}\bigg|_{\omega=\omega_L}, \quad G_{m21} > \frac{1}{|Z_{12}|}\bigg|_{\omega=\omega_M} \tag{3}$$

Looking into port-3, the system can oscillate at either ω_L or ω_H. However, the amplitude of Z_{33} at these frequencies highly depends on the coupling factors k and k'. The values of k and k' cannot be chosen independently. For example, if the inductors L_1 and L_2 are located closer to L_3 to increase k', the value of k would also be increased. Fig. 3(b) illustrates the amplitude of Z_{33} for different values of k and k' (the other resonator parameters are kept constant). By decreasing the coupling between the inductors, the separation of the two resonance peaks decreases and the amplitude of Z_{33} becomes more dominant at ω_H. As a result, by properly setting the negative conductance $-G_{m33}$ in Fig. 2, one can make the oscillator work at ω_H. For a sufficiently large value of G_{m33}, the high-loss mode at ω_L can be also stimulated resulting in simultaneous oscillation at both frequencies. In order to avoid such a behavior, G_{m33} must be chosen such that

$$G_{m33} < \frac{1}{|Z_{33}|}\bigg|_{\omega=\omega_L} \quad \text{and} \quad G_{m33} > \frac{1}{|Z_{33}|}\bigg|_{\omega=\omega_H} \tag{4}$$

On the other hand, for large values of k and k', the lower-frequency peak of $|Z_{33}|$ becomes comparable to its peak at ω_H, hence, the use of just $-G_{m33}$ would result in unstable or even concurrent dual-mode oscillation. However, as previously discussed, the impedance Z_{13} has the same resonance peaks as Z_{33}. Also, the phase response of Z_{13} in Fig. 3(a) shows phase shift of 0° and −180° at ω_L and ω_H, respectively. Thus, by adding two negative transconductances like G_{m31} and G_{m32} in Fig. 2, one can satisfy the oscillation conditions at only ω_H.

Although strongly-coupled inductors are more desirable in terms of chip area, the amplitude of Z_{33} drops for larger values of k and k' (Fig. 3(b)). Thus, the VCO needs to consume more power to achieve the same phase noise performance. In the implemented prototype, to achieve an approximately balanced performance in the three modes,

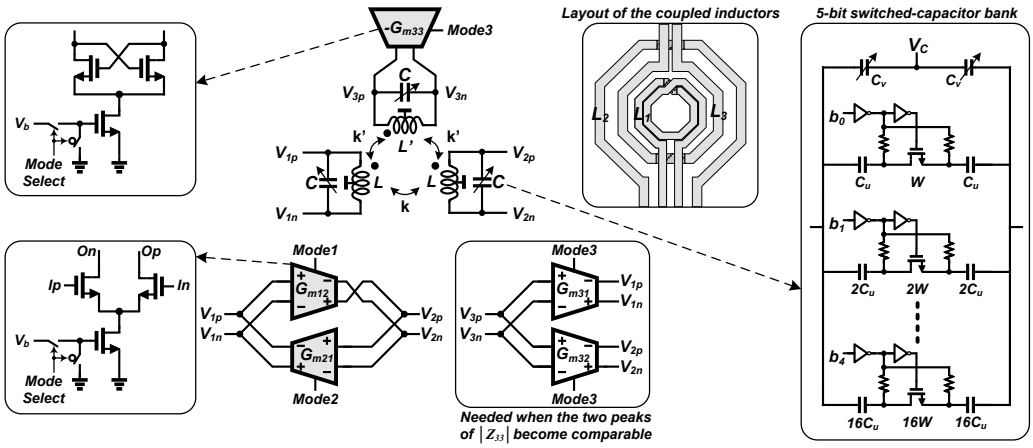

Fig. 2. Detailed schematic of the triple-mode VCO (modes 1, 2 and 3 correspond to oscillation frequencies at ω_L, ω_M and ω_H, respectively).

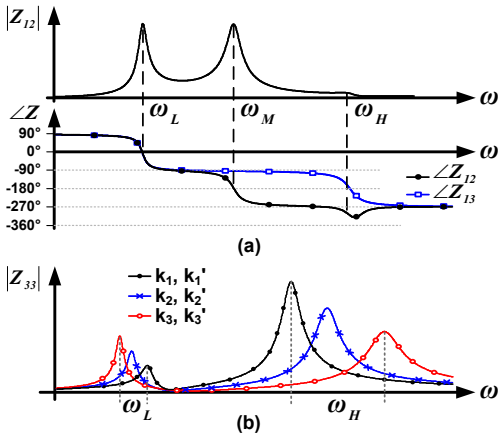

Fig. 3. (a) $|Z_{12}|$ and $\angle Z_{12}$, $\angle Z_{13}$ vs. frequency, and (b) $|Z_{33}|$ vs. frequency for different values of k and k' ($k_1 < k_2 < k_3$, $k'_1 < k'_2 < k'_3$).

the values of k and k' were chosen to be 0.2 and 0.35, respectively. For the designed resonator, simulations verify that the amplitude of Z_{33} is around 10dB larger at ω_H compared to its amplitude at ω_L which was found sufficient to ensure the operation of VCO by using only $-G_{m33}$ even in the presence of worst case PVT variations.

C. Circuit Implementation

As depicted in Fig. 2, the cross-coupled NMOS transistors are used for $-G_{m33}$ while the other G_m-cells are implemented using NMOS differential pairs. A low supply voltage of 1V was chosen to minimize the voltage stress on transistirs. In this way, minimim-length transistors can be used in each G_m-cell which results in less parasitic capacacitance at the outputs of LC tanks. Both coarse and fine tuning are adopted to cover the required frequency range in each mode and to achieve a low VCO gain (K_{VCO}). A Low K_{VCO} reduces AM-PM noise conversion and therefore leads to a better phase noise performance. The coarse frequency tuning is achieved by a 5-bit binary-weighted switched-capacitor bank while the fine tuning is accomplished by small NMOS varactors. The MOS switches are controlled through a 0/1.8V bias and the VCO control voltage (V_C) is tuned from 0 to 1.8V.

The inductive part of the resonator is designed using Sonnet[1] EM simulator. To make $k_{13} = k_{23}$, inductor L_3 is placed between the other two coils (Fig. 2). All inductors are implemented using the top metal layer (M6) in the 0.18µm CMOS process with a thickness of 2µm.

III. Fabrication and Measurements Results

The VCO was fabricated in an IBM 0.18µm CMOS technology with 6 metal layers. A die photo of the chip is shown in Fig. 4. The chip area is 1.3mm×1.5mm with an active core area of 0.33mm^2. The prototype was tested using a GSGSG RF probe and the measurements were conducted with an Agilent E4446A spectrum analyzer.

Fig. 5(a) shows the measured frequency tuning range of the VCO where b<4:0> is the 5-bit control word of the switched-capacitor bank. The VCO is continuously tunable for 5.12-12.95GHz. Also, there is significant overlap between consecutive modes which ensures the operation of VCO at the presence of PVT variations.

Fig. 5(b) shows the measured phase noise at 1MHz offset frequency throughout the tuning range. Fig. 6 shows a sample of measured phase noise curve at 9.12GHz. If the VCO is used with a chain of divide-by-2 circuits, it can provide all the quadrature signals below 6GHz and can meet the stringent phase noise requirements of cellular standards such as GSM/EDGE and WCDMA. The current consumption of the VCO for different modes and across the tuning range has been shown in Fig. 5(c). With reducing frequency in each mode, the tank impedance magnitude drops and hence more current is needed to push the oscillator into the voltage-limited regime. Table I compares this work with recently published wide-tuning range VCOs. The proposed VCO achieves excellent phase

[1]Sonnet Inc. www.sonnet.com

TABLE I

COMPARISON WITH RECENTLY PUBLISHED MULTI-BAND VCOS

	Type	Technology	Supply Voltage (V)	Power (mW)	Freq. (GHz)	Tuning Range	PN (dBc/Hz) @1MHz	FoM (dB)	Area (mm^2)
[4]	Dual-Band	90nm CMOS	1.2	2.2~4.2 /6.7~10	3.1~3.9	23%	-122 @ 2.5MHz	181	0.034
					8.8~11.2	24%	-117 @ 2.5MHz	181.2	
[5]	Dual-Band	65nm CMOS	0.6	9.8~14.2	2.48~3.93	77.5%	-128.3	189.5	0.294
					3.31~5.62		-124.8	186.8	
[6]	Triple-Band	0.13µm CMOS	1.5	4.35~9.15	1.28~2.27	130.2%	-120	177.4	1[1]
					2.34~4.03		-119	181	
					3.65~6.06		-117	181.5	
This Work	Triple-Band	0.18µm CMOS	1	5~10	5.12~7.21	86.7%	-122.9	189.7	0.33
					6.8~10.03		-117	187.5	
					9~12.95		-112	185	

1. Area including pads

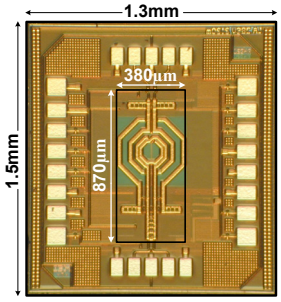

Fig. 4. Die photo of the triple-band VCO.

noise performance as well as competitive FoM [5] compared with the other state-of-the-art designs.

IV. CONCLUSION

A low-phase-noise triple-band VCO is presented for SDR applications based on a resonator with three possible oscillation frequencies. Implemented in 0.18µm CMOS technology, the VCO prototype covers a frequency range of 5.12-12.95GHz and achieves excellent phase noise performance across the whole band.

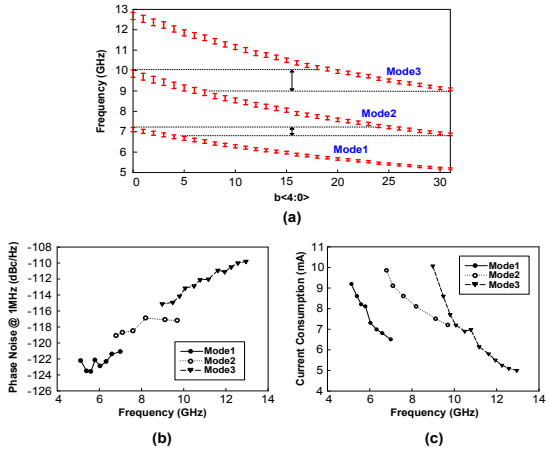

Fig. 5. (a) Measured VCO frequency range, (b) measured phase noise at 1MHz offset frequency, and (c) current consumption across the tuning range.

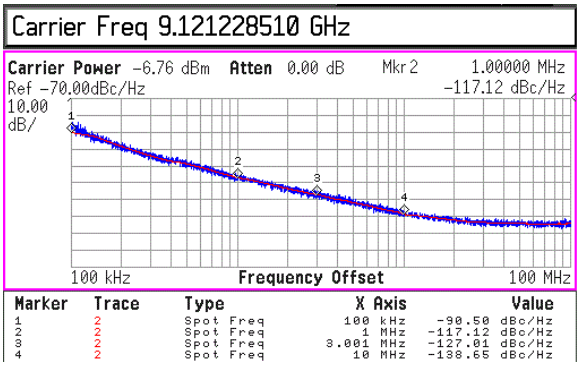

Fig. 6. Measured phase noise at 9.12GHz.

REFERENCES

[1] J. Borremans, K. Vengattaramane, V. Giannini, B. Debaillie, W. V.Thillo, and J. Craninckx, "A 86 MHz–12 GHz digital-intensive PLL for software-defined radios, using a 6 fJ/Step TDC in 40 nm digital CMOS," *IEEE J. Solid-State Circuits*, vol. 45, no. 10, pp. 2116–2129, Oct. 2010.

[2] M. Demirkan, S. P. Bruss, and R. R. Spencer, "Design of wide tuning range CMOS VCOs using switched coupled-inductors," *IEEE J. Solid-State Circuits*, vol. 43, no. 5, pp. 1156–1163, May 2008.

[3] Bevilacqua, F. P. Pavan, C. Sandner, A. Gerosa, and A. Neviani, "A 3.4–7 GHz transformer-based dual-mode wideband VCO," in *Proc. IEEE Eur. Solid-State Circuits Conf. (ESSCIRC)*, pp. 440–443, 2006.

[4] J. Borremans, S. Bronckers, P. Wambacq, M. Kuijk, and J. Craninckx, "A single-inductor dual-band VCO in a 0.06 mm^2 5.6 GHz multi-band front-end in 90 nm digital CMOS," in *IEEE Int. Solid-State Circuits Conf. (ISSCC) Dig.*, pp. 324–325, Feb. 2008.

[5] G. Li, L. Liu, Y. Tang, and E. Afshari, "A Low-Phase-Noise Wide-Tuning-Range Oscillator Based on Resonant Mode Switching," *IEEE J. Solid-State Circuits*, vol. 47, no. 6, pp. 1295-1308, Jun. 2012.

[6] Z. Safarian and H. Hashemi, "Wideband multi-mode CMOS VCO design using coupled inductors," *IEEE Trans. Circuits Syst. I, Reg. Papers*, vol. 56, no. 8, pp. 1830–1843, Aug. 2009.